# AMATH 582 Project: DMD of a weak turbulence

Daniel W. Crews

March 10, 2021

**Abstract**

This project analyzes simulation of a classic problem in collisionless plasma turbulence called the bump-on-tail instability using dynamic mode decomposition (DMD), where spatiotemporally-correlated modes of varying complex frequencies are determined. The bump-on-tail instability describes collisionless relaxation of a superthermal electron beam towards thermodynamic equilibrium. Relaxation occurs through Cherenkov emission of longitudinal plasma waves, leading to a broad distribution of wave energy and a dynamic, weakly turbulent distribution on averaged scales. The problem is solved by evolving the electron distribution function's Boltzmann equation in phase space, setting up its natural observables as the fluid moments projected onto the position and velocity axes. This work pretends not to know about the full phase space information and considers DMD analysis of the observables only, as well as the DMD modes of the Wigner function of spatial wavepackets arising through instability.

## 1 Introduction and Overview

When an experimenter observes a plasma's distribution function they determine an average $\langle f \rangle$ over scales and realizations owing to their instrumentation's resolution. Now consider a numerical experiment wherein one solves microscopic, deterministic equations on some domain with specified initial and boundary conditions. The numerical experimenter obtains a facsimile of the physical experimenter's observations by considering distributions averaged over appropriate scales (such as the domain), effecting a "computational coarse-graining" of time or space scales. In this way the spatially-averaged distribution $\langle f \rangle_x$ and fluid moments $\langle v^n f \rangle_v$ may be considered observable quantities of a simulation of the Vlasov-Poisson systems. Figure 1 shows a schematic overview of the phase space projections as observables associated with phase flow.

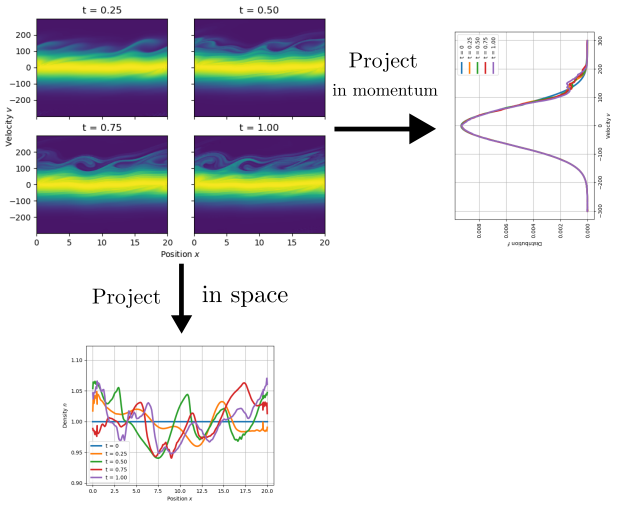


Figure 1: Phase flow is associated natural observable quantities, the mean velocity distribution $\langle f \rangle_v$ and the fluid moments $\langle v^0 f \rangle \equiv n(x)$, $\langle v f \rangle$, $\langle v^2 f \rangle$, etc. Reduced models for collisionless plasma processes attempt to describe dynamics of the projected variables without detailed knowledge of the phase space structure.

# 2 Theoretical Background

## 2.1 Quasilinear weak turbulence theory

The first approximation to velocity-space diffusion in electrostatic turbulence is known as the quasilinear approximation. This basically says that the first approximation to the evolution of the observable distribution $\langle f \rangle_L$ is a heat equation. The reader can skip it. The theory is a reduction from the Vlasov-Poisson equations,

$$\partial_t f + v\partial_x f - \frac{q}{m}\partial_x \varphi \partial_v f = 0, \tag{1}$$

$$\partial_x^2 \varphi(x) = \frac{q}{\epsilon_0}(n_e - n_i), \tag{2}$$

$$n_e \equiv \int_{-\infty}^{\infty} f(v)dv, \quad n_i \equiv \langle n_e \rangle \tag{3}$$

describing collective collisionless behavior as a phase flow conserving probability. Generally one gives a Gaussian initial condition with some perturbation. The average distribution function evolves far from Gaussian during evolution of an instability. If the average wave energy is weak, one can apply quasilinear theory. Here the distribution function is expanded into average and fluctuating parts,

$$f(x,v,t) = f_0(X,v,t) + f_1(x,v,t) \tag{4}$$

$$f_0(X,v,t) = \langle f \rangle_L, \qquad f_1(x,v,t) = f - \langle f \rangle_L, \quad \langle f_1 \rangle_L = 0. \tag{5}$$

In a manner completely analogous to Reynolds averaging, one expands the Vlasov equation, spatially averages, and subtracts the mean to obtain the fluctuating equation,

$$\frac{\partial f}{\partial t} + v\frac{\partial f}{\partial x} + \frac{q}{m}E\frac{\partial f}{\partial v} = 0 \implies \frac{\partial f_0}{\partial t} + \frac{q}{m}\Big\langle \frac{\partial f_1}{\partial v}E_1 \Big\rangle = 0 \tag{6}$$

$$\text{using the averaged equation} \implies \frac{\partial f_1}{\partial t} + v\frac{\partial f_1}{\partial x} + \frac{q}{m}\frac{\partial f_0}{\partial v}E_1 = 0 \tag{7}$$

where in the second equation the variation of the fluctuating force

$$\frac{q}{m}\Big(\frac{\partial f_1}{\partial v}E_1 - \Big\langle \frac{\partial f_1}{\partial v}E_1 \Big\rangle\Big) \tag{8}$$

is considered to be higher-order and dropped for closure, making the evolution of the fluctuation $f_1$ a linear equation whose inhomogeneous part is the flux due to acceleration of the *bulk* distribution [1]. Some remarks are in order on the equation for the background,

$$\frac{\partial f_0}{\partial t} = -\frac{q}{m}\frac{\partial}{\partial v}\langle f_1 E_1 \rangle_L \tag{9}$$

which states that the driver of the observable distribution $f_0 = \langle f \rangle$ is due to the difference in flux $\langle f_1 E_1 \rangle$, or *the unnormalized field-particle correlation coefficient* [2]. The quasilinear closure, dropping Eqn. 8, amounts to supposing that the correlation has zero variance. Under the assumption of linearity of the fluctuation, Fourier transform the equation for $f_1$,

$$\widetilde{f}_1 = -\frac{q}{m}\frac{i}{\omega - kv}\frac{\partial f_0}{\partial v}\widetilde{E}_1 \tag{10}$$

and consider in the continuous spectrum limit $L \to \infty$ the average fluctuating force as

$$\frac{\partial}{\partial v}\Big\langle f_1 E_1 \Big\rangle = \frac{\partial}{\partial v}\Big(\frac{1}{L}\int_0^L f_1 E dx\Big) \approx \frac{\partial}{\partial v}\Big(\frac{1}{L}\int_{-\infty}^{\infty} f_1 E dx\Big) \tag{11}$$

$$= \frac{\partial}{\partial v}\Big(\int_{-\infty}^{\infty}\frac{dk}{2\pi}\frac{\widetilde{E}_1^* \widetilde{f}_1}{L}\Big) \tag{12}$$

where in the last equality Parseval's equality has been used to convert the integrand to spectral variables [1]. Then substitution of $\widetilde{f_1}$ yields

$$\frac{\partial}{\partial v}\Big\langle f_1 E_1 \Big\rangle = -\frac{q}{m}\frac{\partial}{\partial v}\Big( \int_{-\infty}^{\infty} \frac{dk}{2\pi} \frac{\widetilde{E}_1^* \widetilde{E}_1}{L} \frac{i}{\omega - kv} \frac{\partial f_0}{\partial v} \Big) \tag{13}$$

where for causality here $\omega_i > 0$ is taken to have positive imaginary part (a more careful analysis using the Laplace transform arrives at Landau's form for all such resonant integrals). Define the spectral energy density as $\mathcal{E}(k) = \frac{\epsilon_0 \widetilde{E}_1^* \widetilde{E}_1}{2\pi L}$. This form of the correlation closes the equation for the average distribution $f_0$ provided that $\mathcal{E}(k)$ is known. By noting the plasma frequency $\omega_p^2 = \frac{nq^2}{\epsilon_0 m}$, define the diffusion coefficient

$$D(v) = \frac{\omega_p^2}{nm} \int_{-\infty}^{\infty} \frac{i}{\omega - kv} \mathcal{E}(k) dk \tag{14}$$

with which one obtains the *quasilinear diffusion equation* for evolution of $f_0$,

$$\frac{\partial f_0}{\partial t} = \frac{\partial}{\partial v}\Big( D(v) \frac{\partial f_0}{\partial v} \Big). \tag{15}$$

The spectrum $\mathcal{E}(k)$ and dispersion relation $\omega(k) = \omega_r(k) + i\omega_i(k)$ remain to be determined. The simplest equation for evolution of the spectrum follows from trigonometry *assuming no modal interactions* (which take the form of a "collision" term) and slow modulations,

$$\mathcal{E} \sim E^2 \sim e^{2i\omega t} \implies \frac{d\mathcal{E}}{dt} = 2\omega_i \mathcal{E} \tag{16}$$

and for the dispersion relation, one examines the roots of the linear dielectric function,

$$\epsilon(\omega, k) = 1 + \frac{\omega_{pe}^2}{m_e k} \int_{\mathcal{L}} \frac{1}{\omega - kv} \frac{\partial g}{\partial v} dv = 0 \tag{17}$$

where $g = f_e + \sum_s \frac{m_e}{m_s} f_s$ is the unified distribution function which sums over different plasma species. Equations 14 - 17 form a closed, diffusive system to describe the background distribution. However, when an instability saturates the energy is typically larger than the threshold for this purely diffusive approximation to hold true, and other fluctuations are observed. The DMD analysis attempts to see this effect.

## 2.2 Dynamic mode decomposition

In this class, a data matrix was often decomposed into its proper modes using the SVD operation. These frames, such as handwriting examples, were not time-dependent. In simulation of Eqns. 1 and 2, each timestep is separated from its neighbors by a time difference $\Delta t$. If the data is collected into an array $X \in \mathbb{R}^{n \times m}$ of dimension (phase space×time), and a second array $X'$ is formed one difference $\Delta t$ into the future, then the two may be supposed to be related by a Koopman evolution operator,

$$X' = AX \tag{18}$$

where $A$ is taken to solve the problem in the least-squares Moore-Penrose pseudoinverse $Y^+$ sense [3]. However, this makes $A = X'X^+$ a (pixels×pixels) operator. Generally speaking this matrix $A$ will be too large to perform an eigenvalue decomposition on directly with any efficiency. On the other hand, dynamic mode decomposition tackles this problem by projecting into a low-rank truncation of $X$ obtained via SVD,

$$X_r = U_r \Sigma_r V_r^\dagger \tag{19}$$

with $r$ the truncation order. Therefore the Koopman operator $A$ may be represented in this subspace,

$$\widetilde{A} \equiv U_r^\dagger A_r U_r = U^\dagger X' V_r \Sigma_r^{-1} \tag{20}$$

with $\widetilde{A} \in \mathbb{C}^{r\times r}$. Having identified an approximate $A$, a more tractable eigendecomposition is performed

$$\widetilde{A}W = W\Lambda. \tag{21}$$

The orthogonal modes of the low-dimensional evolution operator are then lifted to the full-rank space by

$$\Phi \equiv X' V_r \Sigma_r^{-1} W \tag{22}$$

and the fundamental frequencies computed via $\Omega \equiv \log(\Lambda)/\Delta t$. By this method the DMD has been accomplished according to the approximate continuous-time reconstruction

$$\widetilde{X}(t) = \Phi \exp(\Omega t) b \tag{23}$$

where $b$ is the vector of initial conditions obtained via $b = \Phi^{+} X(0)$. This reconstruction is approximate in the sense that high mode dynamics have been disregarded [4].

# 3 Full simulation results

One way of ensuring the smallness of the terms in Eqn. 8 is that the excited waves are i) small amplitude, e.g. from a weak instability, and ii) are part of a wide family of excited wavenumbers for a continuous range of resonant phase velocities. A problem which fits the conditions of a weakly interacting broad spectrum is called a weak wave turbulence. According to criteria developed in Thorne and Blandford (Ref. [1]), such a distribution is given by a hot distribution drifting through a main Maxwellian's tail,

$$f_0(v) = \frac{1}{(1+\chi)\sqrt{2\pi}} \left[ \frac{1}{v_{t0}} \exp\left( -\frac{v^2}{2v_{t0}^2} \right) + \frac{\chi}{v_{t1}} \exp\left( -\frac{(v-v_b)^2}{2v_{t1}^2} \right) \right] \tag{24}$$

with parameters chosen in the weak turbulence regime with i) bump fraction $\chi = 0.05$, ii) bump spread $v_{t1} = \chi^{1/3} v_b$, and iii) beam velocity $v_b = 5v_{t0}$. The distribution and the growth rates corresponding to Eqn. 17 are shown in Fig. 2. Such a problem is referred to as the bump-on-tail (BOT) instability. The instability can be thought of as the means by which a nonequilibrium distribution releases free energy and relaxes closer to thermal equilibrium through Cherenkov emission mediated by collective interactions.

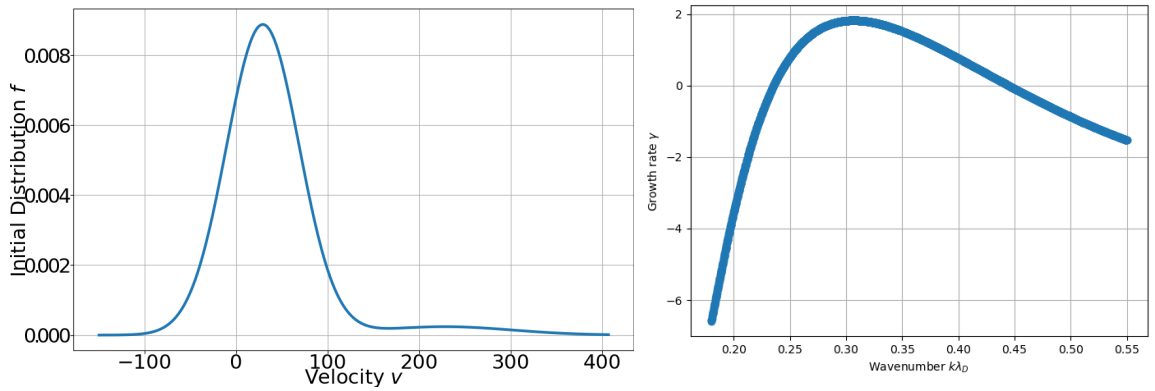


Figure 2: Initial electron distribution $\langle f \rangle_L$ and instability growth rate $\omega_i/\omega_p$ for the bump-on-tail problem. A broad spectrum of Langmuir waves is excited between $k\lambda_D \sim 0.23 - 0.45$.

Figures 3 and 4 show the results of the quasilinear approximation and from direct numerical numerical simulation of the instability, respectively, as well as the Koopman operator's complex frequencies $\omega = \log(\Lambda)/\Delta t$ upon DMD of the observable in the direct simulation. Most modes grow with the instability.

As well, Fig. 6 shows the wavefield of Langmuir waves arising from the instability up to saturation. These wavepackets generically obey a Klein-Gordon type dispersion relation $\omega^2 \sim \omega_p^2 + \langle v^2 \rangle k^2$, which is approximately nonlinear Schrödinger dynamics for these long wavelengths, yet with a growing term.

Further, Fig. 9 shows the complex phase space dynamics occuring during evolution of the instability.

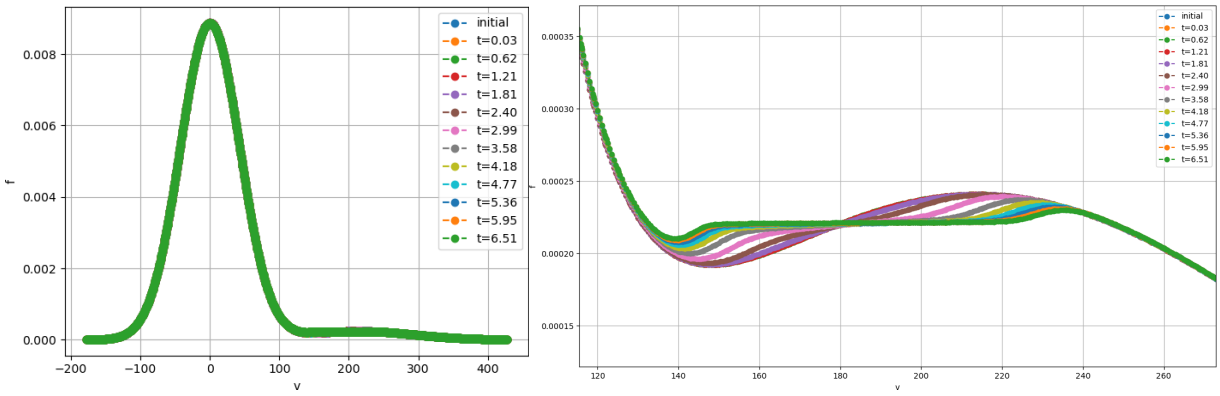


Figure 3: Evolution of bulk distribution $f_0(v)$ (left) and tail flattening (right) in quasilinear approximation of bump-on-tail instability. Approach to the steady-state is necessarily asymptotic.

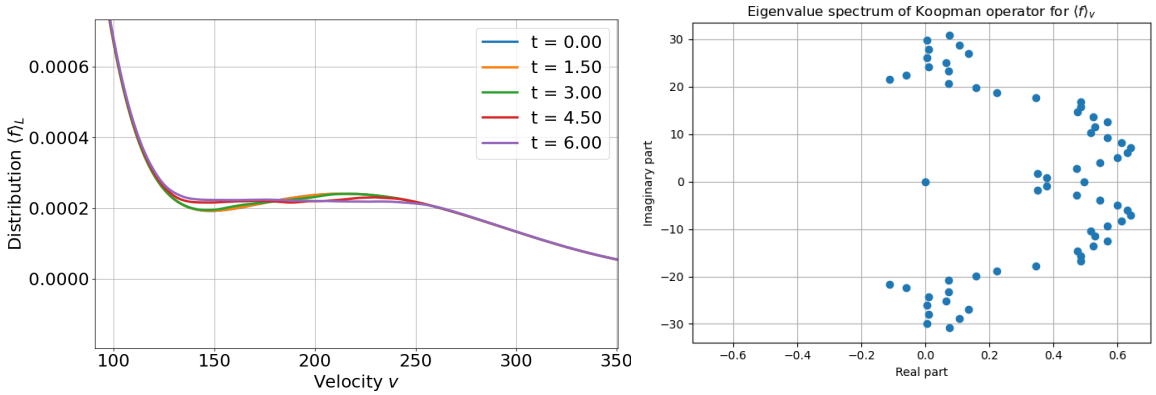


Figure 4: (Left:) Tail flattening of the background $\langle f \rangle_L$ in the electron bump-on-tail instability in a Vlasov-Poisson simulation on $L = 1000\lambda_D$. Observable diffusion proceeds according to quasilinear theory. Important differences are a smaller change in energy of the bulk electrons than in the QL approximation, and a faster rate of smoothing the high-velocity edge. (Right): DMD Koopman complex frequencies of $\langle f \rangle_L$. All parts grow away from the initial condition, which sits squarely at the zero mode occupying a lot of energy.

# 4 Summary and Conclusions

This numerical experiment considered a DMD analysis of the data obtained by direct numerical simulation of a classic plasma instability. Of note was that the eigenvalues of the Koopman operator all grew, indicative of an instability. The resulting spectra were generally not easy to interpret, although the author was surprised by how well the DMD pulled out the background of the observables. More work remains to be done to study the use of DMD to analyze these types of problems.

# References

[1] K.S. Thorne and R.D. Blandford. *Modern Classical Physics.* Princeton, 2018.

[2] N.G. van Kampen. *Stochastic processes in physics and chemistry.* Elsevier, third edition, 2007.

[3] J.N. Kutz. *Data-driven Modeling and Scientific Computation.* Oxford University Press, 1st edition, 2013.

[4] J.N. Kutz. *Dynamic Mode Decomposition.* SIAM, 2016.

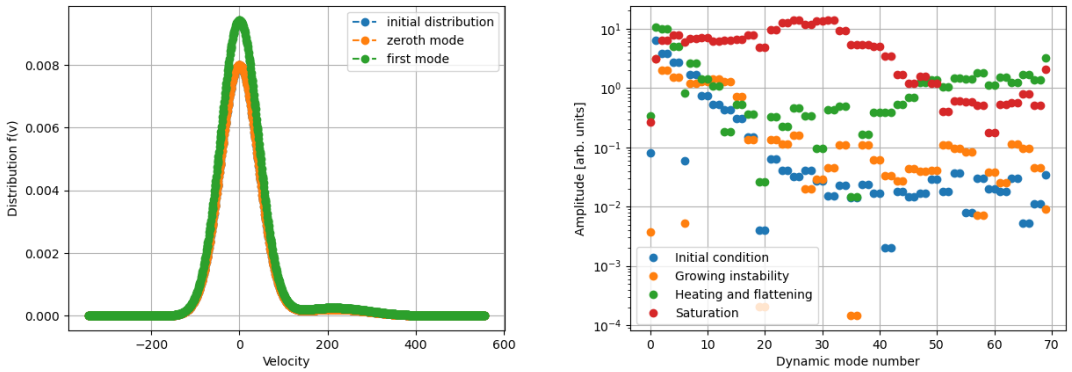


Figure 5: (Left): First DMD modes of $\langle f \rangle$, with the zeroth mode totally overlapping the initial distribution. The larger first mode captures a small change in the background distribution arising due to a small heating of the background distribution due to the instability. (Right): Four snapshots in time of the DMD modal spectrum of $\langle f \rangle$. At saturation, many modes are needed to describe the tail flattening!

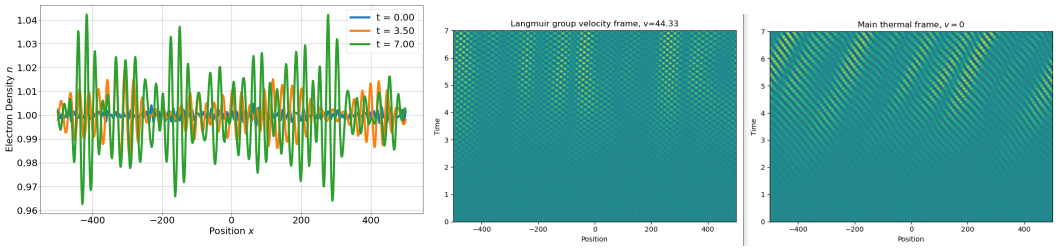


Figure 6: The observable density $n(x)$ at saturation (left) contains a field of wavepackets propagating to the right with the Langmuir group velocity. This translational invariance was removed (right) by a phase shift.

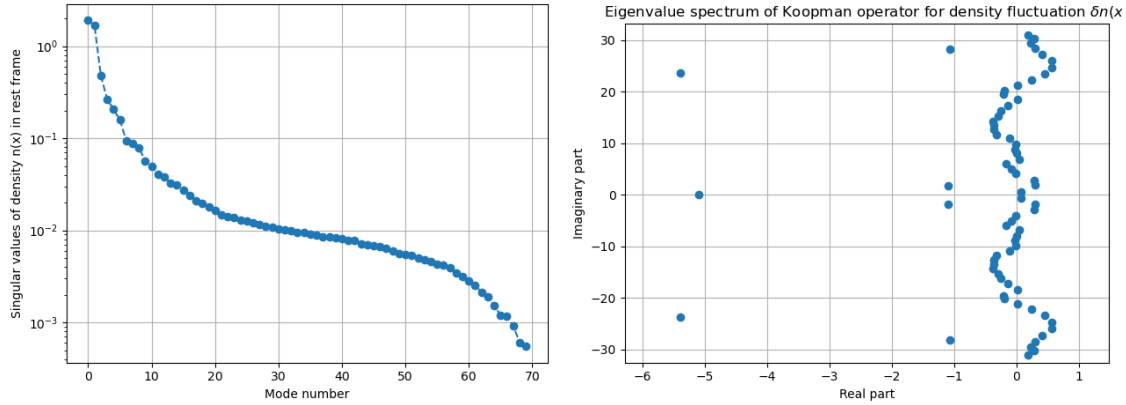


Figure 7: (Left): Singular values of the wavefield after removing translational invariance, which previously was not a sparse spectrum. Instead it is dominated by just two modes. (Right): Complex frequencies of the Koopman operator in DMD of the time-dependent wavefield.

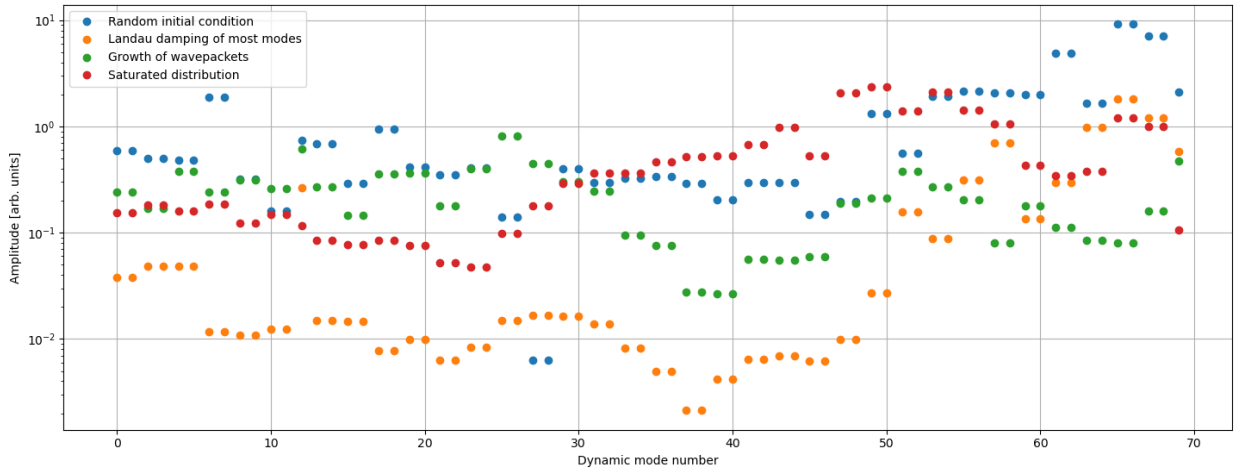


Figure 8: Four time snapshots of the DMD modal spectrum of $\langle f \rangle$, organized by absolute value of the DMD frequency. Initialized by a random wavefield, waves are first damped by collisionless processes, before growing due to the instability. The final spectrum is dominated by the modes which grew, occupying the higher modes seen here.

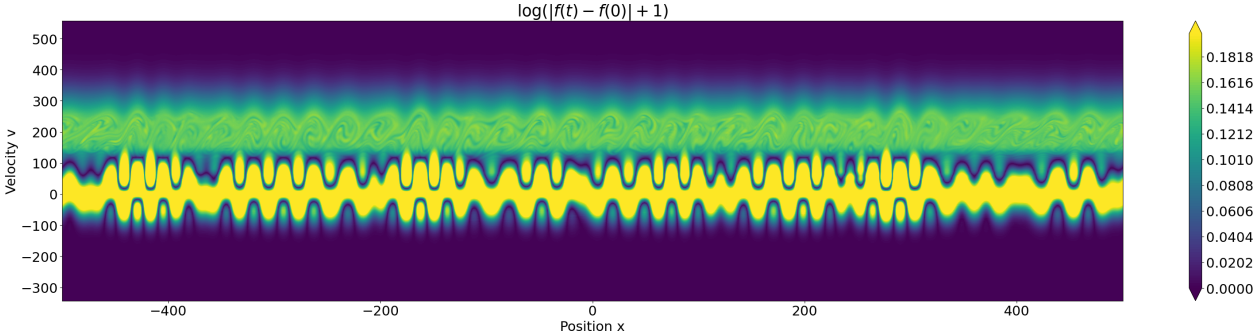


Figure 9: Logarithmic plot of the difference from the initial condition at saturation of the bump-on-tail instability. Highly-correlated wave structures are present, as well as a more chaotic region of particle trapping around the wave phase velocities.